International Journal for
NUMERICAL METHODS IN
FLUIDS

A coupled surface-subsurface model for hydrostatic flows under saturated and variably saturated conditions

Journal:	*International Journal for Numerical Methods in Fluids*
Manuscript ID	FLD-16-0310.R1
Wiley - Manuscript type:	Research Article
Date Submitted by the Author:	n/a
Complete List of Authors:	Casulli, Vincenzo; University of Trento, Civil and Environmental Engineering;
Keywords:	free-surface flow, variable saturated soil, surface-subsurface flow, semi-implicit method, subgrid resolution, mildly nonlinear system

INTERNATIONAL JOURNAL FOR NUMERICAL METHODS IN FLUIDS
Int. J. Numer. Meth. Fluids 2017; **001**:1–18
Published online in Wiley InterScience (www.interscience.wiley.com). DOI: 10.1002/fld

A coupled surface-subsurface model for hydrostatic flows under saturated and variably saturated conditions

Vincenzo Casulli *

Laboratory of Applied Mathematics, Department of Civil, Environmental and Mechanical Engineering, University of Trento, Via Mesiano, 77 – I-38123 Trento, Italy

SUMMARY

In this paper, the governing differential equations for hydrostatic surface-subsurface flows are derived from the Richards and from the Navier-Stokes equations. A vertically integrated continuity equation is formulated to account for both, surface and subsurface flows under saturated and variable saturated conditions. Numerically, the horizontal domain is covered by an unstructured orthogonal grid that may include subgrid specifications. Along the vertical direction a simple z-layer discretization is adopted. Semi-implicit finite difference equations for velocities, and a finite volume approximation for the vertically integrated continuity equation, are derived in such a fashion that, after simple manipulation, the resulting discrete pressure equation can be assembled into a single, two-dimensional, mildly nonlinear system. This system is solved by a nested Newton type method which yields simultaneously the (hydrostatic) pressure and a nonnegative fluid volume throughout the computational grid. The resulting algorithm is relatively simple, extremely efficient and very accurate. Stability, convergence and exact mass conservation are assured throughout also in presence of wetting and drying, in variable saturated conditions, and during flow transition through the soil interface. A few examples illustrate the model applicability and demonstrate the effectiveness of the proposed algorithm. Copyright © 2017 John Wiley & Sons, Ltd.

Received . . .

KEY WORDS: free-surface flow; variable saturated soil; surface-subsurface flow; semi-implicit method; subgrid resolution; mildly nonlinear system

1. INTRODUCTION

The interaction between surface and subsurface water cannot always be neglected, especially at environmental scale where a substantial amount of rainfall is absorbed by the porous soil and later returned to the surface under the gravity force. Environmental flows are characterized by a large horizontal scale and by small vertical extents. Consequently one can reasonably assume *essentially horizontal flows* which imply the validity of the hydrostatic approximation, also known as the Dupuit's assumption [1].

In hydrostatic flows the fluid pressure can be conveniently expressed in terms of the free-surface elevation (or piezometric head) and the two flows, namely the surface flow and the subsurface flow, share the same (hydrostatic) pressure. Consequently the governing differential equations simplify, and very efficient numerical models can be derived to simulate *two-dimensional* flows with high accuracy (see, e.g., [2, 3, 4]).

Simultaneous coupling of surface and saturated subsurface numerical models has been recently extended to *three-dimensional* hydrostatic flows with the remarkable advantage that complex

*Correspondence to: vincenzo.casulli@unitn.it

three-dimensional problems can be solved at a comparable computational cost as required by a corresponding two-dimensional model. This is explained by the fact that in this approach the size and the structure of the discrete pressure equation is essentially two-dimensional and independent from the vertical resolution (see Reference [5] for details).

When the unsaturated subsurface flow has to be included, the governing differential equations are usually formulated by coupling the three-dimensional Richards equation for the subsurface flow, to the two-dimensional shallow water (or further simplified) equations for the hydrostatic overland flow (see, e.g., [6, 7, 8, 9, 10, 11, 12]). Unfortunately, however, Richards equation is known to be computationally demanding and unpredictable because, in general, a solver may easily fail to converge and mass conservation is often inaccurate especially in presence of wetting and drying dynamics, in pressurized flow conditions, in inhomogeneous porous media, and during free-surface transition through the soil interface (see [13]).

In the present investigation an efficient simultaneous coupling strategy for surface and *variably saturated* subsurface flows is proposed. The model being formulated can be regarded as a natural extension of the algorithm presented in Reference [5] that was limited to saturated subsurface flow. Here, assuming the pressure to be in hydrostatic equilibrium, the governing differential equations for the horizontal velocity components are derived from the Richards and from the Navier-Stokes equations, respectively. Moreover, a vertically integrated continuity equation yields an exact differential equation for the (hydrostatic) pressure which closes the system. This equation incorporates the normal velocity boundary condition at the impervious bottom, the kinematic boundary condition at the free-surface and the normal flow continuity at the soil interface.

Numerically, a semi-implicit finite difference method is chosen to approximate the three-dimensional velocity equations [14, 15, 16, 17] and an implicit finite volume method is adopted to approximate the vertically integrated continuity equation [5]. Next, a formal substitution of the unknown horizontal velocities into the discrete vertically integrated continuity equation leads to a *two-dimensional* mildly nonlinear system where the new pressure is the only unknown. This system is iteratively solved by a properly devised converging nested Newton type method [18, 19, 20] which yields, *simultaneously*, the new pressure and the corresponding nonnegative fluid volume on each water column of the horizontal computational grid. Once the new pressure is known, the new horizontal velocities are readily computed from the discrete velocity equations, and the new vertical component of the velocity is recovered recursively from a finite volume approximation of the continuity equation.

The resulting algorithm is relatively simple, extremely accurate, and numerically stable. Moreover, exact mass conservation is assured throughout also in presence of wetting and drying, in variable saturated conditions, and during flow transition through the soil interface. Additionally, when subgrid geometrical details are properly incorporated, then significant improvements of numerical accuracy may be achieved on relatively coarse computational grids (see also [21, 22]).

The remainder of this paper is organized as follows: the governing differential equations are first introduced and discussed in Section 2. In Section 3 the discrete flow variables are defined on a staggered computational grid that may include subgrid specifications. Then, a mildly nonlinear semi-implicit method is proposed in Section 4. In Section 5 a practical solution algorithm is provided. Several hints and remarks are outlined in Section 6 and, finally, in Section 7 this method is applied to some illustrative examples of different surface-subsurface flow problems.

2. THE GOVERNING DIFFERENTIAL EQUATIONS

Within a Cartesian coordinate system (x, y, z) where the x- and y-axis are horizontal and the vertical z-axis is oriented upward along the gravity direction, let $\Omega \subset \mathbf{R}^2$ be the horizontal extent of the flow region being investigated. Moreover, let the vertical extent of the porous material be confined within the interval $[-h(x, y), -s(x, y)]$, where $z = -h(x, y)$ and $z = -s(x, y)$ are surfaces representing the location of the impervious bedrock and the location of the soil surface, respectively (see Figure 1). Of course, $h(x, y)$ and $s(x, y)$ need to be prescribed and must satisfy satisfy $h(x, y) \geq s(x, y)$ for all $(x, y) \in \Omega$.

DOI: 10.1002/fld

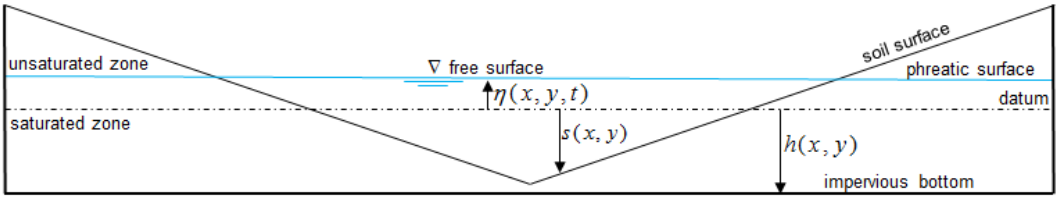

Figure 1. Schematic vertical cross section of an equilibrium flow region

Let the porous material be characterized by a porosity $\epsilon(x,y,z)$ and saturated hydraulic conductivity $\mathcal{K}_s(x,y,z)$ that are prescribed for all $(x,y) \in \Omega$ and for all $z \in [-h(x,y), -s(x,y)]$. For notational convenience the porosity function is prolonged as $\epsilon(x,y,z) = 1$ for all $z \geq -s(x,y)$ and $\epsilon(x,y,z) = 0$ for all $z \leq -h(x,y)$. Additionally, the saturated hydraulic conductivity is prolonged as $\mathcal{K}_s(x,y,z) = 0$ for all $z \notin [-h(x,y), -s(x,y)]$.

Let $u(x,y,z,t)$, $v(x,y,z,t)$ and $w(x,y,z,t)$ be the unknown water velocity components in the x-, in the y- and in the vertical z-direction, respectively; and let $p(x,y,z,t)$ denote the unknown fluid pressure. When the extent of the horizontal domain Ω is much larger than the vertical extent, which is typical in environmental applications, the expected flows are prevalently horizontal and the governing differential equations may be simplified by assuming the pressure to be in hydrostatic equilibrium (see, e.g., [1]). With this assumption (also known as Dupuit's assumption) the unknown piezometric head $\eta(x,y,t)$ is assumed to be independent of the vertical coordinate and the fluid pressure can be expressed in terms of the piezometric head as

$$p(x,y,z,t) = p_a(x,y,t) + \rho g\,[\eta(x,y,t) - z] \tag{1}$$

where t is the time; $p_a(x,y,t)$ is the atmospheric pressure; ρ is the fluid density; and g is the gravitational acceleration. Here, without loss of generality and for notational simplicity, it will be assumed that the atmospheric pressure is $p_a(x,y,t) = 0$ so that sub-atmospheric pressure $p < p_a$ corresponds to $p < 0$. Moreover, the pressure head is linearly decreasing along the vertical direction and is assumed to be $\psi(x,y,z,t) = \eta(x,y,t) - z$.

Note that if $s(x,y) + \eta(x,y,t) > 0$, then the soil within $[-h(x,y), -s(x,y)]$ is assumed to be saturated, and $\eta(x,y,t)$ represents the free-surface elevation of the surface water; alternatively, $s(x,y) + \eta(x,y,t) \leq 0$ indicates the absence of surface water at (x,y), and $\eta(x,y,t)$ represents the phreatic surface of the subsurface water (see Figure 1). In all cases the unknown function $\eta(x,y,t)$ represents the local (hydrostatic) pressure.

2.1. *Governing equations for sub-surface flow*

The governing equations for the horizontal water velocities in the saturated subsurface domain were originally derived by Darcy and later generalized to the unsaturated zone by Richards [23]. These equations are given by

$$\begin{cases} u = -\mathcal{K}\frac{\partial \eta}{\partial x} \\ v = -\mathcal{K}\frac{\partial \eta}{\partial y} \end{cases} \tag{2}$$

where $\mathcal{K} = \mathcal{K}(x,y,z,\eta)$ is a nonnegative hydraulic conductivity which can also be expressed as $\mathcal{K} = \frac{\rho g \kappa}{\mu}$, where $\kappa(x,y,z,\eta)$ is the so called soil permeability, ρ is the fluid density and μ is a dynamic viscosity coefficient.

The continuity equation governing the flow in variably saturated porous media is called Richards' equation, and can be written as

$$\frac{\partial \theta}{\partial t} + \frac{\partial u}{\partial x} + \frac{\partial v}{\partial y} + \frac{\partial w}{\partial z} = 0 \tag{3}$$

DOI: 10.1002/fld

where $\theta(x,y,z,\eta)=\epsilon(x,y,z)S(x,y,z,\eta)$ is the moisture content, and $S=S(x,y,z,\eta)$ is the water saturation. Clearly, the saturation is nonnegative and bounded everywhere and at all times. Specifically, $0\le S(x,y,z,\eta)\le 1$. Consequently, the moisture content $\theta(x,y,z,\eta)$ is itself nonnegative and bounded. Specifically, $0\le\theta(x,y,z,\eta)\le\epsilon(x,y,z)$.

Some of the most commonly used constitutive relationships relating the saturation $S(x,y,z,\eta)$ and the hydraulic conductivity $\mathcal{K}(x,y,z,\eta)$ to the piezometric head $\eta(x,y,t)$ will be outlined in Section 2.4.

The differential Equations (2)–(3) are the model equations that describe the water flow within the subsurface three-dimensional domain identified by $(x,y)\in\Omega$ and $-h(x,y)<z<-s(x,y)$.

2.2. *Governing equations for surface flow*

The Navier-Stokes equations expressing the horizontal momentum balance for surface flow, account for inertia, pressure, and viscous forces. When the pressure is assumed to be in hydrostatic equilibrium as given by Equation (1), these equations (see, e.g., [5]) can be written as

$$\left\{\begin{array}{l}\frac{\partial u}{\partial t}+u\frac{\partial u}{\partial x}+v\frac{\partial u}{\partial y}+w\frac{\partial u}{\partial z}=-g\frac{\partial\eta}{\partial x}+\frac{\partial}{\partial x}\left(\nu\frac{\partial u}{\partial x}\right)+\frac{\partial}{\partial y}\left(\nu\frac{\partial u}{\partial y}\right)+\frac{\partial}{\partial z}\left(\nu\frac{\partial u}{\partial z}\right)\\ \frac{\partial v}{\partial t}+u\frac{\partial v}{\partial x}+v\frac{\partial v}{\partial y}+w\frac{\partial v}{\partial z}=-g\frac{\partial\eta}{\partial y}+\frac{\partial}{\partial x}\left(\nu\frac{\partial v}{\partial x}\right)+\frac{\partial}{\partial y}\left(\nu\frac{\partial v}{\partial y}\right)+\frac{\partial}{\partial z}\left(\nu\frac{\partial v}{\partial z}\right)\end{array}\right. \tag{4}$$

where $\nu(x,y,z,t)\ge 0$ is a prescribed kinematic viscosity coefficient. The boundary conditions associated to Equations (4) at the bottom and at the free-surface are assumed to be

$$\left.\begin{array}{l}\nu\frac{\partial u}{\partial z}=\gamma u^*\\ \nu\frac{\partial v}{\partial z}=\gamma v^*\end{array}\right\}\text{at } z=-s,\qquad \left.\begin{array}{l}\nu\frac{\partial u}{\partial z}=0\\ \nu\frac{\partial v}{\partial z}=0\end{array}\right\}\text{at } z=\eta$$

where $\gamma(x,y,t)$ is a non-negative bottom friction coefficient, and u^* and v^* are the horizontal velocity components near the soil interface.

The continuity equation governing the surface flow, expressing mass conservation, is the well-known incompressibility condition which can be written as

$$\frac{\partial u}{\partial x}+\frac{\partial v}{\partial y}+\frac{\partial w}{\partial z}=0 \tag{5}$$

The differential Equations (4)–(5) are the model equations that describe the water flow within the surface three-dimensional domain identified by $(x,y)\in\Omega$ and $-s(x,y)<z<\eta(x,y,t)$.

At the initial time $t_0=0$ the surface velocities $u(x,y,z,0)$, $v(x,y,z,0)$ and $w(x,y,z,0)$ are prescribed as initial conditions. The initial fluid position is specified by prescribing the piezometric head $\eta(x,y,0)$ for all $(x,y)\in\Omega$.

2.3. *The vertically integrated continuity equation*

At any point within the subsurface region the saturation $S(x,y,z,\eta)$ is prescribed as function of the piezometric head η by an appropriate constitutive relationship. The saturation is prolonged to the surface region as $S(x,y,z,\eta)=\mathcal{H}(\eta-z)$, where $\mathcal{H}$ is the Heaviside step function which is *one* when its argument is strictly positive and *zero* otherwise. Consequently, for all $(x,y)\in\Omega$ and $z>-s(x,y)$ one has $\theta(x,y,z,\eta)=S(x,y,z,\eta)=\mathcal{H}(\eta-z)$.

Recall that at any point $(x,y)\in\Omega$, if $s(x,y)+\eta(x,y,t)>0$, then the unknown function $\eta(x,y,t)$ represents the free-surface elevation and the soil within the interval $[-h(x,y),-s(x,y)]$ is saturated. On the other hand, if $s(x,y)+\eta(x,y,t)\le 0$ then the surface layer is dry, Equations (4) do not apply, and $\eta(x,y,t)$ represents the phreatic surface of the subsurface wet region.

In all cases, by setting $\beta(x,y,t)=\max\left[\eta(x,y,t),-s(x,y)\right]$, one has $\theta(x,y,z,\eta)=0$ for all $z\notin[-h(x,y),\beta(x,y,t)]$. Thus, the total moisture content over the entire water column, which accounts for both the surface and the subsurface water, can be defined as $\Theta(x,y,\eta)=\int_{-h}^{\beta}\theta(x,y,z,\eta)\,dz$.

Now, integration of the continuity equations (3) and (5) along the vertical z-direction, after simple manipulations, yields

DOI: 10.1002/fld

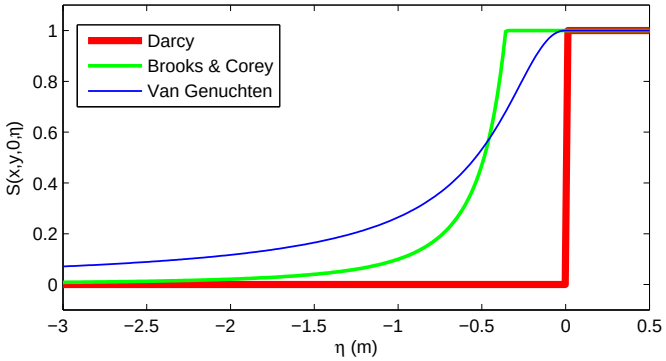

Figure 2. Saturation curves for the Darcy, the Brooks and Corey, and for the van Genuchten model

$$\frac{\partial \Theta}{\partial t} + \frac{\partial}{\partial x}\left(\int_{-h}^{\beta} u\, dz\right) + \frac{\partial}{\partial y}\left(\int_{-h}^{\beta} v\, dz\right) = 0 \tag{6}$$

Equation (6) is a two-dimensional vertically integrated continuity equation expressing an *exact* mass balance over the entire water column for all $(x, y) \in \Omega$ and for all $t > 0$. This is a key equation that links the piezometric head $\eta(x, y, t)$ to both, surface and subsurface velocities.

Moreover, it can be shown that in addition to the normal velocity boundary condition at the impervious bottom, and the kinematic boundary condition at the free-surface, Equation (6) also incorporates the normal flow continuity at the soil interface between the surface and the subsurface flow regions.

2.4. *Constitutive relationships*

In order to complete the model within the subsurface domain one needs to specify the constitutive relationships relating the saturation $S(x, y, z, \eta)$ and the hydraulic conductivity $\mathcal{K}(x, y, z, \eta)$ to the piezometric head $\eta(x, y, t)$. In general, at any point (x, y, z) the functions $S(x, y, z, \eta)$ and $\mathcal{K}(x, y, z, \eta)$ are assumed to be nonnegative, non decreasing, and bounded functions of η. Here, three of the most commonly employed models, namely the Darcy's model [5], the Brooks–Corey model [24] and the van Genuchten model [25], are outlined (see Figure 2).

In the Darcy's model the unsaturated zone is neglected and the porous media is assumed to be either fully saturated or completely dry. Accordingly, the saturation $S(x, y, z, \eta)$ and the hydraulic conductivity $\mathcal{K}(x, y, z, \eta)$ are binary functions. Specifically,

$$S(x, y, z, \eta) = \begin{cases} 0 & \text{if} \quad \eta \leq z \\ 1 & \text{if} \quad \eta > z \end{cases} \tag{7}$$

$$\mathcal{K}(x, y, z, \eta) = \mathcal{K}_s S \tag{8}$$

In this case Equation (3) simplifies to yield velocity divergence free and the model Equations (2)–(6) reduce to the one recently presented in Reference [5].

Alternatively, the constitutive relationships may also account for variably saturated porous media. Thus, for example, the model proposed by Brooks and Corey [24] allows the porous material to be fully saturated or variably saturated depending on the local value of the piezometric head. In this case $S(x, y, z, \eta)$ and $\mathcal{K}(x, y, z, \eta)$ are taken to be

DOI: 10.1002/fld

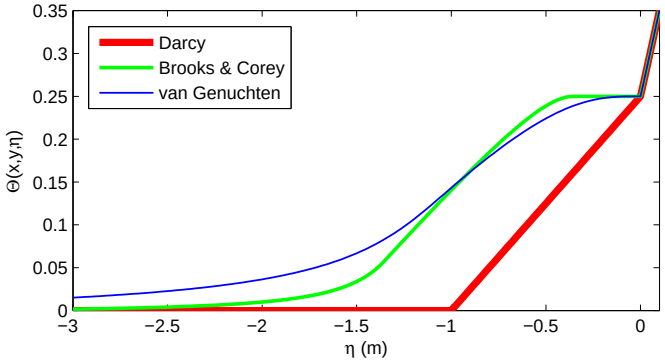

Figure 3. Vertically integrated moisture content

$$S(x,y,z,\eta) = \begin{cases} [\alpha(z-\eta)]^{-n} & \text{if} \quad \eta \le z - \frac{1}{\alpha} \\ 1 & \text{if} \quad \eta > z - \frac{1}{\alpha} \end{cases} \tag{9}$$

$$\mathcal{K}(x,y,z,\eta) = \mathcal{K}_s S^{3+\frac{2}{n}} \tag{10}$$

where $\alpha(x,y,z) > 0$ and $n(x,y,z) \ge 1$ are material parameters which affect the shape of the soil hydraulic functions.

The most commonly employed constitutive relationships, proposed by van Genuchten [25] to provide a smoother transition from the fully saturated to a variable saturated region, are given by

$$S(x,y,z,\eta) = \begin{cases} \left\{1 + [\alpha(z-\eta)]^n\right\}^{-m} & \text{if} \quad \eta \le z \\ 1 & \text{if} \quad \eta > z \end{cases} \tag{11}$$

$$\mathcal{K}(x,y,z,\eta) = \mathcal{K}_s \sqrt{S} \left[1 - \left(1 - \sqrt[m]{S}\right)^m\right]^2 \tag{12}$$

where, again, $\alpha(x,y,z) > 0$ and $n(x,y,z) \ge 1$ are prescribed material parameters, and $m = 1 - \frac{1}{n}$.

Figure 3 illustrates the resulting vertically integrated moisture content curves $\Theta(x,y,\eta)$ for the three models given above in the very simple case $h(x,y) = 1$, $s(x,y) = 0$, and constant porosity distribution $\epsilon(x,y,z) = 0.25$ for all $z \in [-1,0]$. In this case $\Theta(x,y,\eta)$ grows nonlinearly when $\eta(x,y,t) \le 0$ and it grows linearly with slope 1 when $\eta(x,y,t) > 0$. In general, $\Theta(x,y,\eta)$ is always a nonnegative and non decreasing function of η.

Equations (7)-(12) constitute three basic and well-known models which relate the saturation and the hydraulic conductivity to the piezometric head. The numerical method being proposed in the present investigation is not restricted to these three models. In more realistic situations other constitutive relationships may be specified to account, e.g., for specific storativity, pressurized flows, fluid temperature, soil freezing, etc. In general, the prescribed saturation $S(x,y,z,\eta)$ and the hydraulic conductivity $\mathcal{K}(x,y,z,\eta)$ need to be nonnegative, non decreasing, and bounded functions of η.

3. UNSTRUCTURED GRID AND SUBGRID

In order to solve Equations (2)–(6) numerically, the region Ω is covered by an *unstructured orthogonal grid* consisting of a set of non-overlapping convex polygons Ω_i, $i = 1, 2, ..., N_p$ separated by N_s sides Γ_j, $j = 1, 2, \ldots, N_s$. Within each polygon a *center* must be identified in

DOI: 10.1002/fld

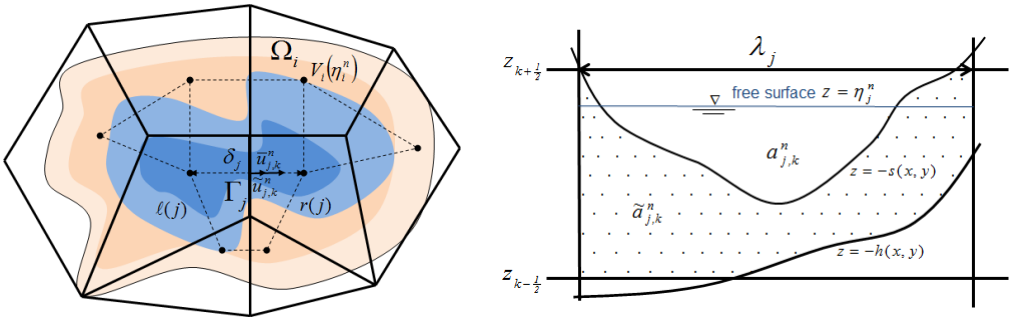

Figure 4. Discrete flow variables on a staggered orthogonal grid: plan view and vertical cross section

such a way that the segment joining the centers of two adjacent polygons and the side shared by the two polygons, have a non empty intersection and are *orthogonal* to each other (see Reference [17] for further details).

Once Ω has been covered with an unstructured orthogonal grid, each polygon Ω_i may have an arbitrary number of sides. Let S_i denote the set of sides of the ith polygon. The left and the right polygons which share the jth internal side are identified by the indices $\ell(j)$ and $r(j)$, respectively.

Moreover, let $\wp(i,j)$ denote the neighbor of polygon i that shares side j with the ith polygon. The nonzero distance between the centers of two adjacent polygons which share the jth internal side is denoted with δ_j and the length of each side is denoted by $\lambda_j,\ j = 1, 2, ..., N_s$.

Along the vertical direction a simple finite difference discretization, not necessarily uniform, is adopted. Thus, by denoting with $z_{k+\frac{1}{2}}$ a given level surface, the vertical discretization step is defined by $\Delta z_k = z_{k+\frac{1}{2}} - z_{k-\frac{1}{2}},\ \ k = 1, 2, \ldots, N_z$. Hence, the three-dimensional space discretization consists of prisms whose horizontal faces are the polygons at two consecutive level surfaces, and whose height is Δz_k (see Figure 4).

The discrete piezometric head η_i^n at time level t_n, assumed to be constant over each polygon, is located at the center of the ith polygon and the corresponding non-negative fluid *volume* within the ith water column is given by

$$V_i(\eta_i^n) = \int_{\Omega_i} \Theta(x, y, \eta_i^n) d\Omega_i \tag{13}$$

For any prescribed piezometric head $\eta_i^n,\ i = 1, 2, \ldots, N_p$, a value for η_j^n along each internal edge Γ_j is derived from the nearest grid values by taking, e.g., the average, the upwind, or the maximum between $\eta_{\ell(j)}^n$ and $\eta_{r(j)}^n$.

The nonnegative *subsurface wet area* of each vertical face of the computational grid is given by

$$\tilde{a}_{j,k}^n = \int_{\Gamma_j} \int_{z_{k-\frac{1}{2}}}^{z_{k+\frac{1}{2}}} \mathcal{H}\left(\mathcal{K}(x, y, z, \eta_j^n)\right) d\Gamma\, dz \tag{14}$$

and satisfies $0 \le \tilde{a}_{j,k}^n \le \lambda_j \Delta z_k$.

Likewise, the *surface wet area* of each vertical face is taken to be

$$\bar{a}_{j,k}^n = \int_{\Gamma_j} \int_{z_{k-\frac{1}{2}}}^{z_{k+\frac{1}{2}}} \mathcal{H}\left(\theta(x, y, z, \eta_j^n)\right) \left[1 - \mathcal{H}\left(\mathcal{K}(x, y, z, \eta_{j,k}^n)\right)\right] d\Gamma\, dz \tag{15}$$

and satisfies $0 \le \bar{a}_{j,k}^n \le \lambda_j \Delta z_k$. Moreover, the total face wet area satisfies $\tilde{a}_{j,k}^n + \bar{a}_{j,k}^n \le \lambda_j \Delta z_k$.

On each vertical face with a non zero subsurface wet area (i.e., $\tilde{a}_{j,k}^n > 0$), the face averaged hydraulic conductivity is taken to be

DOI: 10.1002/fld

$$\mathcal{K}^n_{j,k} = \frac{1}{\tilde{a}^n_{j,k}} \int_{\Gamma_j} \int_{z_{k-\frac{1}{2}}}^{z_{k+\frac{1}{2}}} \mathcal{K}(x,y,z,\eta^n_j) d\Gamma \, dz \tag{16}$$

Finally, the effective jth edge lengths available to surface water are given by

$$\lambda^n_{j,k+\frac{1}{2}} = \int_{\Gamma_j} \mathcal{H}\left(\min(\eta^n_j, z_{k+\frac{1}{2}}) + s(x,y)\right) d\Gamma \tag{17}$$

and satisfies $0 \le \lambda^n_{j,k+\frac{1}{2}} \le \lambda_j$.

The surface and subsurface horizontal velocities perpendicular to each wet vertical face of the computational grid, are assumed to be constants over the face and are denoted with $\bar{u}^n_{j,k}$ and $\tilde{u}^n_{j,k}$, respectively. The positive direction for $\bar{u}^n_{j,k}$ and $\tilde{u}^n_{j,k}$ is chosen to go from $\ell(j)$ to $r(j)$. Similarly, the discrete surface and subsurface vertical velocities are assumed to be constants over each wet horizontal face of the computational grid, and are denoted with $\bar{w}^n_{i,k\pm\frac{1}{2}}$ and $\tilde{w}^n_{i,k\pm\frac{1}{2}}$, respectively.

Note that *only* the discrete velocities $\tilde{u}^n_{j,k}$, $\bar{u}^n_{j,k}$, $\tilde{w}^n_{i,k\pm\frac{1}{2}}$ and $\bar{w}^n_{i,k\pm\frac{1}{2}}$, and the discrete piezometric heads η^n_i, are defined and assumed to be constant at their respective staggered locations. Geometrical structures such as impervious bottom $h(x,y)$, soil surface $s(x,y)$ and soil porosity $\epsilon(x,y,z)$, as well as the saturated hydraulic conductivity $\mathcal{K}_s(x,y,z)$ and the material parameters $\alpha(x,y,z)$ and $n(x,y,z)$, can be prescribed everywhere with sufficient *subgrid* resolution in order to allow an accurate evaluation of the integrals appearing in (13)-(17) and best fitting of rugged topography. To this purpose, if necessary, all integrals in (13)-(17) can be evaluated numerically by any standard quadrature formula in order to include valuable subgrid details with the desired accuracy.

4. FINITE DIFFERENCE – FINITE VOLUME APPROXIMATION

Equations (2)–(6) will be discretized on an unstructured orthogonal grid by using finite difference approximations for the velocity Equations (2) and (4), and a finite volume approximation for the vertically integrated continuity Equation (6).

4.1. Finite difference approximation for subsurface horizontal velocities

The Darcy's Equations (2) do not contain time derivatives, thus they must be satisfied at each time level. These equations are invariant under solid rotation of the x- and y-axis on the horizontal plane. Hence, within the subsurface flow region, and with a properly oriented coordinate system, a simple linear *finite difference* approximation for Equations (2) is taken to be

$$\tilde{u}^{n+1}_{j,k} = -\mathcal{K}^n_{j,k} \frac{\eta^{n+1}_{r(j)} - \eta^{n+1}_{\ell(j)}}{\delta_j}, \qquad k = \tilde{m}_j, \tilde{m}_j + 1, \ldots, \tilde{M}^n_j \tag{18}$$

where $\tilde{m}_j$ and $\tilde{M}^n_j$ denote the lowest and the highest nonempty subsurface vertical face, respectively. As indicated $\tilde{m}_j$ and $\tilde{M}^n_j$ depend on their spatial location j, and $\tilde{M}^n_j$ may also change with the time level t_n.

Of course, Equation (18) is defined only on wet vertical faces, *i.e.*, where $\tilde{a}^n_{j,k} > 0$. On dry faces $\tilde{u}^{n+1}_{j,k} = 0$ is assumed. Thus, for each unknown subsurface velocity $\tilde{u}^{n+1}_{j,k}$, one has exactly one linear Equation (18).

4.2. Finite difference approximation for surface horizontal velocities

Any explicit numerical method for solving Equations (4)-(6) for surface flows would be simple but limited by a rather severe stability restriction on the time step size. On the other hand, a fully implicit discretization of these equations may lead to methods which are unconditionally stable. Fully implicit methods, however, at every time step would require the simultaneous solution of a large number of coupled nonlinear equations.

DOI: 10.1002/fld

With a *semi-implicit* method the terms to be discretized at the new time level are carefully selected in order to obtain a stable method with a minimal computational effort [14, 15, 16, 17]. Specifically, the advective and the horizontal viscosity terms of the momentum Equations (4) are discretized explicitly, whereas the pressure gradient in the momentum Equations (4), and the velocities in the vertically integrated continuity Equation (6) are discretized implicitly. Moreover, the vertical viscosity and the wall friction are taken implicitly. Thus, since Equations (4) are invariant under solid rotation of the x- and y-axis on the horizontal plane, a consistent semi-implicit *finite-difference* discretization for the momentum Equations (4) is taken to be

$$\begin{aligned}\bar{a}^n_{j,k}\bar{u}^{n+1}_{j,k} &= \bar{a}^n_{j,k}F\bar{u}^n_{j,k} - g\Delta t\,\bar{a}^n_{j,k}\frac{\eta^{n+1}_{r(j)}-\eta^{n+1}_{\ell(j)}}{\delta_j} - \Delta t\,\gamma^n_{j,k}(\lambda^n_{j,k+\frac{1}{2}}-\lambda^n_{j,k-\frac{1}{2}})\bar{u}^{n+1}_{j,k}\\ &+ \Delta t\left(\lambda^n_{j,k+\frac{1}{2}}\nu^n_{j,k+\frac{1}{2}}\frac{\bar{u}^{n+1}_{j,k+1}-\bar{u}^{n+1}_{j,k}}{\Delta z_{k+\frac{1}{2}}} - \lambda^n_{j,k-\frac{1}{2}}\nu^n_{j,k-\frac{1}{2}}\frac{\bar{u}^{n+1}_{j,k}-\bar{u}^{n+1}_{j,k-1}}{\Delta z_{k-\frac{1}{2}}}\right)\\ &\qquad k=\bar{m}_j,\bar{m}_j+1,\ldots,\bar{M}^n_j \qquad (19)\end{aligned}$$

where F is any stable non-linear difference operator that includes a spatial discretization of the advective and horizontal viscous terms; Δt is the time step size; $\gamma^n_{j,k}$ is a nonnegative wall friction coefficient; and $\bar{m}_j$ and $\bar{M}^n_j$ denote the lowest and the highest nonempty surface vertical face, respectively. As indicated $\bar{m}_j$ and $\bar{M}^n_j$ depend on their spatial location j, and $\bar{M}^n_j$ may also change with the time level t_n in order to account for the free-surface dynamics. Clearly, $\bar{a}^n_{j,k} > 0$ for all $k=\bar{m}_j,\bar{m}_j+1,\ldots,\bar{M}^n_j$; moreover $\lambda^n_{j,m_j-\frac{1}{2}}=0$ and $\lambda^n_{j,k+\frac{1}{2}}-\lambda^n_{j,k-\frac{1}{2}}\geq 0$ for all $k=\bar{m}_j,\bar{m}_j+1,\ldots,\bar{M}^n_j$; and the wind stress at the free-surface is neglected by setting $\bar{u}^{n+1}_{j,\bar{M}^n_j+1}=\bar{u}^{n+1}_{j,\bar{M}^n_j}$.

A particular form for F in Equation (19) can be chosen in a variety of ways, such as by using an Eulerian-Lagrangian scheme [14, 15, 16, 17], or an explicit conservative formulation [26]. Since this topic is widely covered in the literature, a specific formulation for obtaining $F\bar{u}^n_{j,k}$ will not be elaborated in the present study. Here, we only insist that F be a *stable* operator in the sense that if F is only conditionally stable, then that stability condition will extend as the stability condition required by the method being developed [16]. As an example, when an Eulerian-Lagrangian discretization is used, a form for F is taken to be

$$F\bar{u}^n_{j,k} = \bar{u}^L_{j,k} + \Delta t\Delta_h\bar{u}^L_{j,k}$$

where $\bar{u}^L_{j,k}$ denotes the velocity component normal to the jth side of the grid interpolated at time t_n at the end of the Lagrangian trajectory. The Lagrangian trajectory is calculated by integrating the velocity backwards in time from node (j,k) at t_{n+1} to its location at time t_n. Finally, $\Delta_h\bar{u}^L_{j,k}$ is an explicit discretization of the horizontal viscosity terms (see, e.g., [17, 22] for further details).

Of course, Equation (19) is defined only on wet vertical faces, *i.e.*, where $\bar{a}^n_{j,k} > 0$. On dry faces $\bar{u}^{n+1}_{j,k}=0$ is assumed. Thus, for any structure given to F, one has exactly one linear Equation (19) for each unknown surface velocity $\bar{u}^{n+1}_{j,k}$.

4.3. *Finite volume approximation for the vertically integrated continuity equation*

Finally, in order to close the system, a consistent discretization of the vertically integrated continuity Equation (6) in flux form is obtained upon integration of Equation (6) over the ith polygon. This yields the following implicit *finite volume* approximation

$$V_i(\eta^{n+1}_i) = V_i(\eta^n_i) - \Delta t\sum_{j\in S_i}\sigma_{i,j}\left(\sum_{k=\tilde{m}_j}^{\tilde{M}^n_j}\tilde{a}^n_{j,k}\tilde{u}^{n+1}_{j,k} + \sum_{k=\bar{m}_j}^{\bar{M}^n_j}\bar{a}^n_{j,k}\bar{u}^{n+1}_{j,k}\right) \qquad (20)$$

Prepared using fldauth.cls
DOI: 10.1002/fld

where $V_i(\eta_i^{n+1})$ and $V_i(\eta_i^n)$ are the new and the previous water volumes within the ith water column, and $\sigma_{i,j}$ is a sign function associated with the orientation of the normal velocities defined on the jth vertical faces. Specifically,

$$\sigma_{i,j} = \frac{r(j) - 2i + \ell(j)}{r(j) - \ell(j)}$$

The discrete continuity Equation (20) expresses an exact mass balance regardless of the piezometric heads η_i^n and η_i^{n+1}. This equations, however, is *mildly nonlinear* and the nonlinearity resides in the definition of the fluid volume $V_i(\eta_i^{n+1})$ given by Equation (13).

Equation (20) applies to each water column identified by the corresponding polygon Ω_i. Thus, one has exactly one Equation (20) for each unknown piezometric head $\eta_i^{n+1},\ i = 1, 2, \ldots, N_p$.

All together, Equations (18), (19) and (20) constitute a mildly nonlinear system of at most $2N_sN_z + N_p$ equations. This large system has to be solved at each time step in order to determine the new field variables $\tilde{u}_{j,k}^{n+1}$, $\bar{u}_{j,k}^{n+1}$ and η_i^{n+1} throughout the computational grid.

5. SOLUTION ALGORITHM

The system of $2N_sN_z + N_p$ equations formed by (18)-(20) can be conveniently decomposed into a reduced *mildly nonlinear* system of N_p equations for η_i^{n+1}; at most N_sN_z *explicit* equations for the subsurface horizontal velocities $\tilde{u}_{j,k}^{n+1}$; and a set of N_s independent *linear* tridiagonal systems of at most N_z equations for the surface horizontal velocities $\bar{u}_{j,k}^{n+1}$. Specifically, Equations (18)-(19) and (20) are first written in vector notation as

$$\tilde{\mathbf{u}}_j^{n+1} = -\mathbf{K}_j^n \frac{\eta_{r(j)}^{n+1} - \eta_{\ell(j)}^{n+1}}{\delta_j} \tag{21}$$

$$\mathbf{A}_j^n \bar{\mathbf{u}}_j^{n+1} = \mathbf{G}_j^n - g\Delta t \frac{\eta_{r(j)}^{n+1} - \eta_{\ell(j)}^{n+1}}{\delta_j} \bar{\mathbf{a}}_j^n \tag{22}$$

$$V_i(\eta_i^{n+1}) = V_i(\eta_i^n) - \Delta t \sum_{j \in S_i} \sigma_{i,j} \left[\left(\tilde{\mathbf{a}}^\top\right)_j^n \tilde{\mathbf{u}}_j^{n+1} + \left(\bar{\mathbf{a}}^\top\right)_j^n \bar{\mathbf{u}}_j^{n+1} \right] \tag{23}$$

where $\tilde{\mathbf{u}}_j^{n+1}$ and $\bar{\mathbf{u}}_j^{n+1}$ are vectors containing the unknown subsurface velocities $\tilde{u}_{j,k}^{n+1}$ and the surface velocities $\bar{u}_{j,k}^{n+1}$, respectively; $\mathbf{K}_j^n$ is a vector containing the hydraulic conductivities $\mathcal{K}_{j,k}^n$; $\mathbf{A}_j^n$, is a symmetric, positive definite, tridiagonal matrix that includes bottom friction and vertical viscosity terms; $\tilde{\mathbf{a}}_j^n$ and $\bar{\mathbf{a}}_j^n$ are vectors whose entries are the vertical face areas $\tilde{a}_{j,k}^n$ and $\bar{a}_{j,k}^n$, respectively; and $\mathbf{G}_j^n$ is a vector containing the known explicit terms in Equation (19).

Formal substitution of $\tilde{\mathbf{u}}_j^{n+1}$ and $\bar{\mathbf{u}}_j^{n+1}$ from (21) and (22) into (23) yields the following discrete pressure equation

$$V_i(\eta_i^{n+1}) - \Delta t \sum_{j \in S_i} \left\{ \left[\left(\tilde{\mathbf{a}}^\top \mathbf{K}\right)_j^n + g\Delta t \left(\bar{\mathbf{a}}^\top \mathbf{A}^{-1} \bar{\mathbf{a}}\right)_j^n \right] \frac{\eta_{\wp(i,j)}^{n+1} - \eta_i^{n+1}}{\delta_j} \right\} = b_i^n \tag{24}$$

where b_i^n is given by

$$b_i^n = V_i(\eta_i^n) - \Delta t \sum_{j \in S_i} \sigma_{i,j} \left(\bar{\mathbf{a}}^\top \mathbf{A}^{-1} \mathbf{G}\right)_j^n$$

Equations (24) can be assembled into a sparse, *mildly nonlinear* system of N_p equations with N_p unknowns η_i^{n+1}, $i = 1, 2, \ldots, N_p$. This system has a symmetric, and at least positive semi-definite Jacobian matrix. Nevertheless, since the volume functions $V_i(\eta)$ are neither concave nor convex (see Figure 3), a straightforward application of the classical Newton method could easily lead to undefined or non converging iterations [13]. For this reason the use of a nested Newton

DOI: 10.1002/fld

type method described in Reference [20] is advised because, in this case, convergence can always be assured under rather general assumptions on the soil properties and geometric details (see also [5, 13, 19, 27]).

Once the new piezometric heads η_i^{n+1} have been determined, the discrete subsurface velocities $\tilde{\mathbf{u}}_j^{n+1}$ are readily determined from Equations (21). Additionally, Equations (22) now constitute a set of N_s *linear*, tridiagonal systems with at most N_z equations each. All these systems are independent from each other, symmetric and positive definite. Thus, they can be conveniently solved by a direct method to uniquely determine the horizontal surface velocities $\bar{\mathbf{u}}_j^{n+1}$.

In summary, assuming the knowledge of $\tilde{u}^n$, $\bar{u}^n$ and η^n from the previous time level t_n, each time step is advanced by preliminarily determining the volumes $V(\eta^n)$, the wet areas $\tilde{a}^n$ and $\bar{a}^n$, the face averaged hydraulic conductivities $\mathcal{K}_{j,k}^n$ and the wet lengths λ^n from (13)–(17). Then the mildly nonlinear system (24) is assembled and solved iteratively to obtain *simultaneously* the new piezometric heads η^{n+1} and the corresponding fluid volumes $V(\eta^{n+1})$; next, the new subsurface velocities $\tilde{u}^{n+1}$ are readily determined from Equation (21); the discrete horizontal velocities $\bar{u}^{n+1}$ are obtained as solution of the N_s linear tridiagonal Systems (22); and, finally, the new vertical components of the velocity $\tilde{w}^{n+1}$ and $\bar{w}^{n+1}$ are diagnostically derived from a finite volume approximation of the continuity Equations (3) and (5), respectively (see, e.g., [5]).

6. HINTS AND REMARKS

It can be shown that the stability of the semi-implicit method (18)-(20) remains independent of the celerity, wall friction and vertical viscosity (see [16]). The stability does depend on the discretization of the advection and horizontal viscosity terms. In other words, when F is stable, then the resulting discrete model (18)-(20) is also stable.

It should be noted that, the size and the structure of the mildly nonlinear System (24) is independent from the vertical resolution and from the prescribed subgrid details. Subgrid, and vertical resolution affect the assembly of Equation (24) and the number of equations for horizontal and vertical velocities. Moreover, since a major part of the computational effort is required to determine the piezometric heads from Equations (24), a detailed subgrid data and a fine vertical resolution can be adopted with an acceptable increase of the corresponding computational effort.

On the other hand, if only one vertical layer is specified ($N_z = 1$), then Equations (18)-(20) simplify to a consistent approximation for the coupled surface-subsurface model governed by the two-dimensional shallow water equations for the surface flow, and by the two-dimensional vertically averaged Richards equation for the subsurface flow. A one-dimensional model is also obtained from the present formulation by further arranging the unstructured orthogonal grid in such a fashion that each polygon Ω_i has at the most two neighbors.

Additionally, if the soil level coincides with the impervious bottom everywhere, then only surface flow is allowed and can be solved by the present method as a particular case. This particular case was reported in Reference [22]. Similarly, if $s(x, y) + \eta(x, y, t) \leq 0$ for all $(x, y) \in \Omega$ and for all $t > t_0$, then the surface region remains dry and only subsurface flow is being solved by the present method as another particular case (see [20]).

Furthermore, when the simplest Darcy's constitutive relationships (7)–(8) are adopted to relate saturation and hydraulic conductivity to the piezometric head, then the unsaturated flow is neglected and the present method simplifies to the one recently presented in Reference [5].

More importantly, when this method is applied to environmental flow domains which are often characterized by complex geometries, then each section of the flow region gets its own correct representation without artificial treatments at the interfaces.

The proposed method, whose general formulation has been presented above in its simplest form, can be further modified to simulate a variety of specific surface-subsurface problems. As an example, sources and/or sinks can be included by simply allowing a nonzero right hand side to the continuity Equations (3) and (5). Also, additional forces such as Coriolis or baroclinic pressure can be considered by including appropriate terms to the velocity Equations (2) and (4). An additional

DOI: 10.1002/fld

advection diffusion equation may also be included to model the transport of scalar variables such as salinity, water temperature and/or contaminants [28].

7. NUMERICAL TESTS

The accuracy, the efficiency and the robustness of the proposed method for simulating *subsurface* flows in confined-unconfined aquifers has been shown in [13, 18, 19, 20]. The applicability of this method to simulate *surface* flow problems within a subgrid environment has been already documented in [21, 22, 29, 30]. Also, examples of coupled surface-subsurface flows under *saturated* conditions have been recently reported in Reference [5] and will not be duplicated here.

In this section the applicability the above method is briefly shown on a few illustrative test cases where the interaction of surface and subsurface flows includes the *unsaturated* zone. Specifically, the first test case concerns a one-dimensional flow and water exchange between a tidal basin and an adjacent lagoon through an interposed sandy embankment; in a second test, salinity intrusion in a coastal aquifer along with density stratification that develops in the coastal area is simulated; and, finally, surface and subsurface runoff flows resulting from a long-lasting rainfall on a V-shaped catchment basin are simulated.

The proposed method has been implemented in a single, general purpose computer code which includes options for scalar transport, for baroclinic and for non hydrostatic pressure. The specific momentum advection operator that is used for these test cases is an Eulerian-Lagrangian extension of the explicit conservative scheme discussed in Reference [26]. Moreover, the bottom friction coefficient adopted in these specific tests is assumed to be $\gamma = g\frac{\sqrt{(u^*)^2+(v^*)^2}}{C_z^2}$, where C_z is the Chezy's bed roughness coefficient.

In every run the system of pressure Equations (24) is solved to machine accuracy in order to obtain a precise mass conservation. In all tests the qualitative aspects of the computed results will be emphasized. All calculations have been performed on a laptop with an Intel i7 CPU having $2.60\,GHz$ clock frequency and $16\,GB$ of RAM.

7.1. Flow in a tidal lagoon

In this first test the flow and water exchange between an idealized tidal basin and an adjacent lagoon is simulated. Detailed observations and measurements of an experimental groundwater transport through the sand embankment between the wetland and the coastal area have been reported in Reference [31]. The tidal basin and the lagoon are separated by a trapezoidal sandy embankment characterized by a constant porosity $\epsilon = 0.3$ and saturated hydraulic conductivity $\mathcal{K}_s = 0.01\,m/s$. The one-dimensional horizontal flow region is $\Omega = [-L, L]$ where $L = 2.64\,m$. As illustrated in Figure 5, a constant depth is set to $h(x) = 0$ and the trapezoidal sandy embankment is prescribed by specifying $s(x) = min\left[0, max\left(-0.33, \frac{1}{2}|x - 1.04| - 0.35\right)\right]$.

At the initial time $t_0 = 0$ the flow is at rest and the prescribed initial piezometric head is set to $\eta(x, t_0) = 0.274\,m$ everywhere. Then a no flow boundary condition is specified at the right boundary as $u(L, t) = 0$, and a periodic (tidal) boundary condition on the free-surface elevation is prescribed at the left boundary as $\eta(-L, t) = 0.214 + a\,cos(2\pi t/T)$, where $T = 355\,s$ is the tidal period and $a = 0.06\,m$ is the tidal amplitude.

This problem has been studied with various models using different coupling strategies [3, 4, 5, 9]. Here, for the surface flow the horizontal viscosity is neglected ($\nu = 0$) and the Chezy's bed roughness coefficient is taken to be $C_z = 50\,m/s$. Moreover, the Brooks and Corey constitutive relationships (9)-(10) are used with constant soil parameters given by $\alpha = 29\,m^{-1}$ and $n = 4$.

Numerically, the horizontal domain Ω is covered with $N_p = 264$ uniform segments Ω_i of length $\delta_j = 2\,cm$ and the vertical resolution is limited to only one vertical layer. The simulation for this *one-dimensional* test problem is carried on for 10 tidal cycles requiring 710 time steps with a time step size $\Delta t = 5\,s$. The elapsed computing time to complete the entire simulation is only $T_{cpu} = 20\,s$.

The computed saturation at low tide and at high tide is shown in Figure 5. The red line across the sandy embankment indicates the computed piezometric head and the vertical distribution of the

DOI: 10.1002/fld

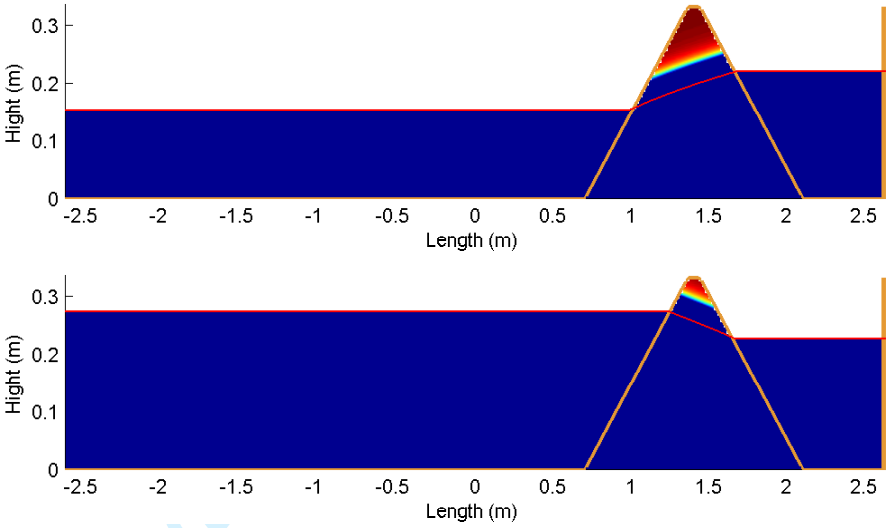

Figure 5. Computed saturation and piezometric heads at low tide and at high tide

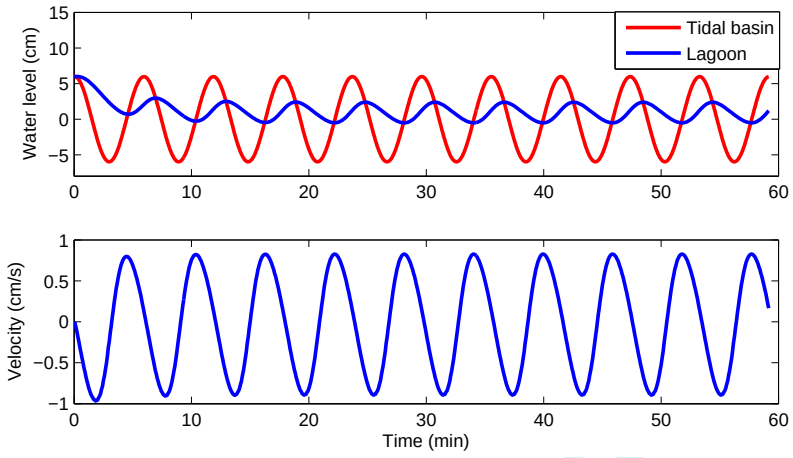

Figure 6. Tidal fluctuation at both sides of the sandy embankment and velocity time series in the tidal basin

saturation is thereby derived from the constitutive relationship (9). Figure 6 shows the time series for the water level relative to the mean sea level in the tidal basin and in the lagoon, respectively. The water surface oscillation in the lagoon has a near 90^0 phase lag compared with the tidal oscillation, and the average water level in the lagoon is higher than that in the tidal basin. Figure 6 also shows the velocity time series computed at $x_s = -0.56\,m$. These results are in excellent agreement with the observations [31] and with previously computed results [3, 4, 5, 9, 31].

7.2. *Salt water intrusion into a coastal aquifer*

The management of saltwater intrusion into coastal aquifers is one of the most challenging environmental management problems faced by water resource planners worldwide [32]. The flow driving salt water intrusion into groundwater aquifers may be assumed to be hydrostatic and yet, the vertical velocity, though small, has to be sufficiently resolved in order to simulate both, the groundwater salt-wedge and surface water stratification. In this test the experimental results reported in Reference [32] are reproduced after extending the computational domain to include an equal surface region where the development of surface water stratification is expected. Additionally, in

DOI: 10.1002/fld

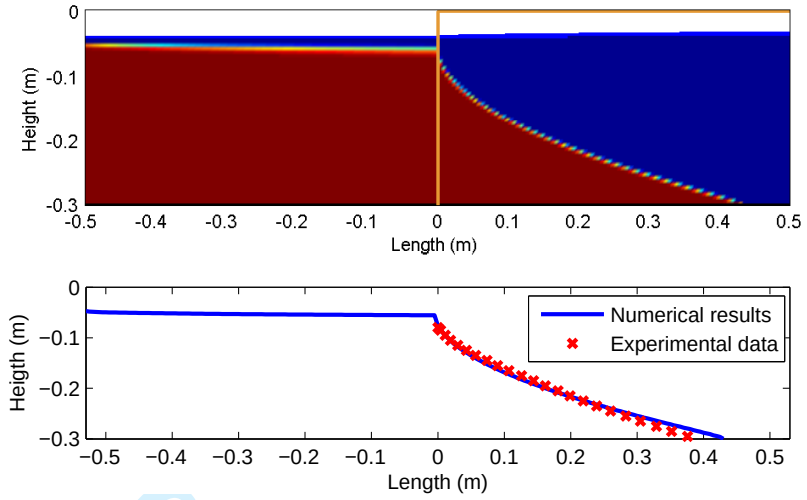

Figure 7. Computed fresh water stratification and salt wedge (top), and the $5\,ppt$ isochlor (bottom)

order to simulate the expected density flow, a baroclinic pressure gradient term has been added to the velocity Equations (2) and (4), and the associated advection-diffusion equation for salinity has been solved by a conservative finite volume method detailed in Reference [28].

The one-dimensional horizontal flow domain is $\Omega = [-L, L]$, with $L = 53\,cm$, and is equally divided into a surface region located in $[-L, 0]$, and a subsurface domain located in $[0, L]$. A constant depth is set to $h(x) = 0.3\,m$ and the soil surface is prescribed by specifying $s(x) = 0.3\,\mathcal{H}(-x)$ (see Figure 7).

The aquifer is characterized by a constant porosity $\epsilon = 0.385$ and saturated hydraulic conductivity $\mathcal{K}_s = 105\,m/day$. Here, for the surface flow the viscosity coefficient is taken to be $\nu = 10^{-3}\,m^2/s$ and the Chezy's bed roughness coefficient is chosen as $C_z = 50\,m/s$. Moreover, the unsaturated zone is neglected by adopting the simple Darcy constitutive relationships (7)-(8).

At the initial time $t_0 = 0$ the flow is at rest and the prescribed initial piezometric head is set to $\eta(x, t_0) = -4.5\,cm$ for $x < 0$, and $\eta(x, t_0) = -3.8\,cm$ for $x > 0$. Additionally, the initial salt concentration is set to $c(x, z, 0) = 10\,\mathcal{H}(-x)\,ppt$. Thereafter the piezometric heads and salinity concentrations at both boundaries are maintained constants. Specifically, $\eta(-L, t) = -4.5\,cm$, $\eta(L, t) = -3.8\,cm$, $c(-L, z, t) = 10\,ppt$, and $c(L, z, t) = 0\,ppt$ for all $t > 0$.

Numerically, the horizontal domain Ω is covered with uniform segments of length $\delta_j = 0.5\,cm$ thereby resulting in $N_p = 212$ control volumes for each vertical layer. Additionally, the vertical dimension of total height $H = 30\,cm$ is discretized with $N_z = 60$ vertical layers having uniform thickness $\Delta z_k = 0.5\,cm$. Thus this is a *two-dimensional* simulation in the vertical (x, z) plane.

This simulation is carried to steady state for 100 000 time steps using a small time step of size $\Delta t = 0.05\,s$ until a final time $T = 5\,000\,s$ is reached. The size of the mildly nonlinear System (6) being solved at every time step is N_p and is independent from the vertical resolution N_z. The elapsed computing time to reach steady state is $T_{cpu} = 1\,800\,s$. Figure 7 shows the computed piezometric heads, the fresh water stratification developed in the salty surface area, and the salt wedge developed within the aquifer. Having included a surface flow region, the resulting solution in this test case is more comprehensive and is not expected to exactly mach the experimental measurements that were limited to the subsurface region. Nevertheless, these results show an excellent match between the observations reported in Reference [32] and previously computed results in the subsurface region [32, 33, 34].

7.3. Surface-subsurface flow in a V-shaped catchment

In this last test both, surface and subsurface runoff flows resulting from a long-lasting rainfall are simulated in a V-shaped catchment basin. The spatial domain includes an overland region, a

DOI: 10.1002/fld

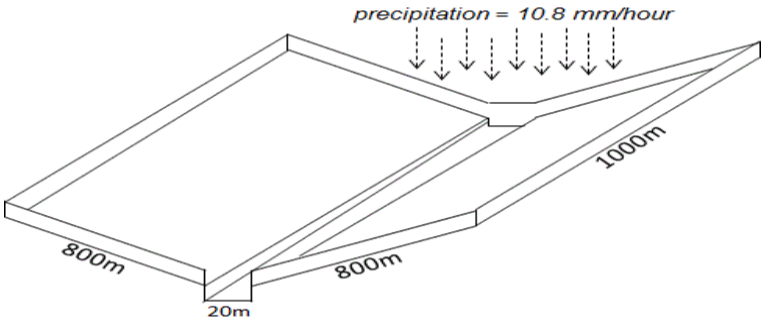

Figure 8. Soil surface in a V-shaped catchment basin

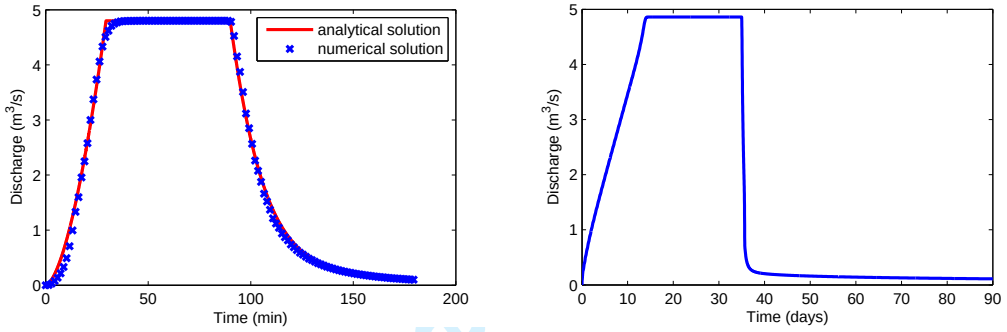

Figure 9. Computed channel outflow

channel and a subsurface region characterized by a homogeneous soil with constant porosity $\epsilon = 0.1$ and constant saturated hydraulic conductivity $\mathcal{K}_s = 5 \times 10^{-5} m/s$. For the surface flow the fluid viscosity is neglected ($\nu = 0$) and the Chezy's bed roughness coefficient is taken to be $C_z = 10\, m/s$ [5]. Moreover, the van Genuchten constitutive relationships (11)-(12) with constant soil parameters $\alpha = 1\, m^{-1}$ and $n = 1.4$ are used.

The flow domain Ω consists of a $1000\, m \times 1620\, m$ slope which includes a $1000\, m$ long channel of width $20\, m$. The depth of the channel has a slope $s_c = 0.02$ and varies from $0\, m$ at the upstream end to $20\, m$ at the downstream end, whereas the surface slope is $s_s = 0.05$ in the transversal direction perpendicular to the channel [35]. Thus, assuming that the origin is located at the center of Ω, the soil level is given by $s(x, y) = -0.05|x|$ for all $(x, y) \in \Omega$ and $|x| \geq 10\, m$; and $s(x, y) = 10 - 0.02y$ for all $(x, y) \in \Omega$ and $|x| < 10\, m$ (see Figure 8). The underlying aquifer extends from the soil surface to a constant depth $h(x, y) = 20\, m$ for all $(x, y) \in \Omega$. This problem has received considerable attention in the recent literature where different sets of governing equations and various numerical methods have been tested (see, e.g., [5, 6, 7, 10, 11, 12, 35]).

The flow region Ω is covered with a total of $N_p = 4\,050$ uniform squares Ω_i with $\lambda_j = \delta_j = 20\, m$, and only one vertical layer is considered. Thus, the governing equations being solved are the *two-dimensional* vertically averaged Richards equation for the subsurface flow and the two-dimensional shallow water equations for overland and channel flows.

At the initial time $t_0 = 0$ the fluid is at rest with a constant piezometric head $\eta(x, y, t_0) = 0$ so that the initial surface water is confined within the channel. A no flow boundary condition is applied everywhere except at at the downstream end of the channel where the water level is maintained to be $\eta(x, y, t) = 0\, m$ for all times $t > t_0$. The flow is generated by a rainfall event with a rainfall rate $r = 10.8\, mm/hour$ which is applied everywhere in Ω for all $t \in [0, t^*]$, and with *zero* rainfall for all $t \in [t^*, T]$.

For validation purpose in a first run the subsurface region is ignored by setting $h(x, y) = s(x, y)$ for all $(x, y) \in \Omega$ and, after setting $t^* = 90\, min$, the simulation is carried on for $8\,640$ time steps with

DOI: 10.1002/fld

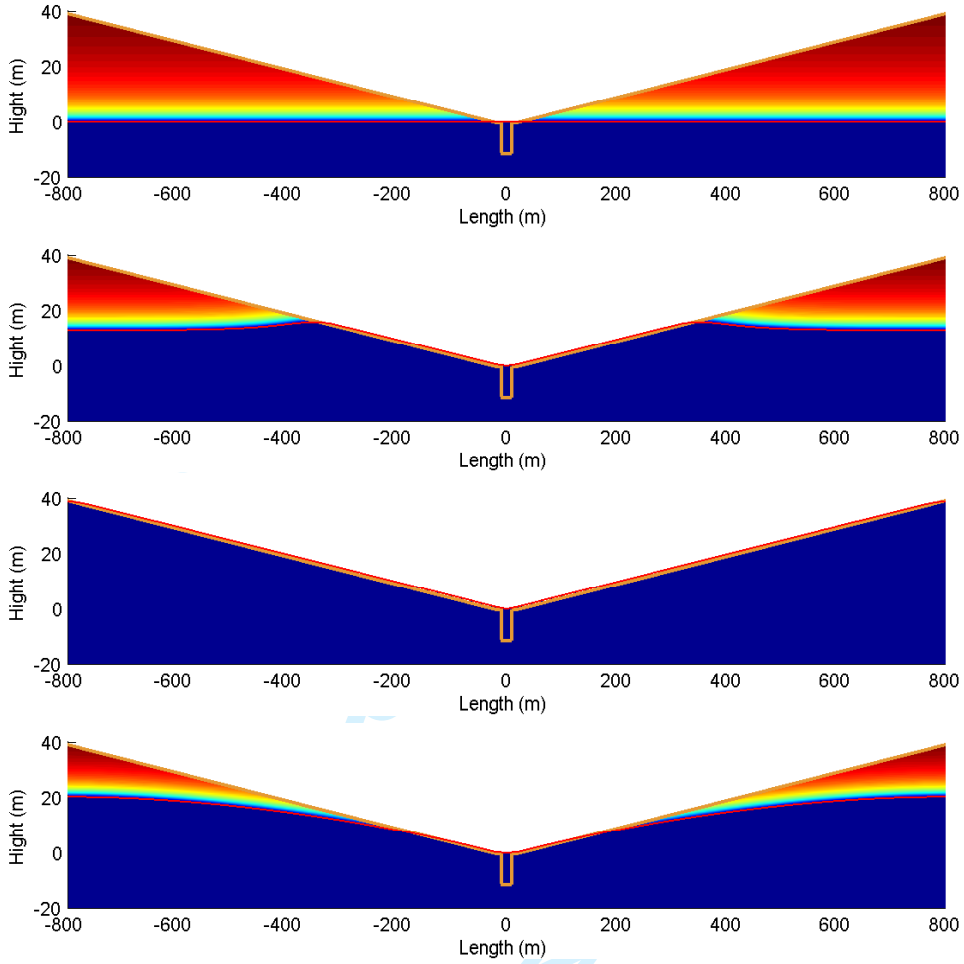

Figure 10. Cross section saturation profiles at $t = 0$, $t = 5\,days$, $t = 15\,days$, and $t = 90\,days$

a time step size $\Delta t = 1.25\,s$ until the final time $T = 180\,min$ is reached. As expected, Figure 9 (left) shows an excellent agreement between the resulting outflow hydrograph and the analytical solution of a simplified kinematic model for surface runoff response [35].

Next, after including the subsurface region, a new simulation of a long-lasting rainfall event with $t^* = 35\,days$ is carried on for 6 480 time steps with a large time step size $\Delta t = 20\,min$ until the final time $T = 90\,days$ is reached. Figure 9 (right) shows the resulting outflow hydrograph indicating a gradually rising limb while water is being stored within the porous soil. Then a steady outflow balances the rainfall while the soil remains fully saturated until $t = 35\,days$. Thereafter a receding limb continues for long time at a gradually declining rate as the stored groundwater drains to the channel. The elapsed computing times to complete this simulation is $T_{cpu} = 3\,456\,s$, which is less than $1\,hour$ for a $90\,days$ simulation.

Figure 10 shows the time evolution of the water saturation at a cross section through the center of Ω and perpendicular to the drainage channel. The red line indicates the computed piezometric head separating the unsaturated from the underlying saturated region.

8. CONCLUSIONS

The governing differential equations for velocities are derived from the Richards and from the Navier-Stokes equations under the assumption of hydrostatic flow. A conservative form of the

DOI: 10.1002/fld

vertically integrated continuity equation expresses an exact mass balance over the entire water column in terms of both, the surface and subsurface horizontal integral fluxes.

Numerically, an unstructured orthogonal grid, possibly including subgrid details, is chosen to cover the entire flow domain with the desired spatial resolution. Then an implicit finite difference approximation of the Darcy's laws provides a linear relationship between the horizontal subsurface velocities and the unknown piezometric heads. Likewise, an appropriate semi-implicit finite difference approximation of the momentum equations provides a linear relationship between the horizontal surface velocities and the unknown piezometric heads. Finally, the vertically integrated continuity equation is approximated by a conservative implicit method to express an exact mass balance in terms of the total horizontal fluxes over the entire water column.

From the computational point of view, a formal substitution of the unknown velocities into the discrete pressure equation leads to a well posed mildly nonlinear system where the new piezometric heads are the only unknowns. This reduced system is solved iteratively and yields, *simultaneously*, the new piezometric heads and the corresponding fluid volume on each water column. Finally, the horizontal velocities are readily computed from the discrete velocity equations.

The resulting method is extremely efficient and the time step size is not restricted by a stability conditions dictated by surface wave speed, wall friction or vertical viscosity. Moreover, for any time step size the computed fluid volumes are assured to be everywhere nonnegative and exact mass conservation is guaranteed also in presence of wetting and drying, in variable saturated conditions, and during flow transition through the soil interface. A few computational examples show the applicability of the proposed method to a variety of surface-subsurface flow problems.

REFERENCES

1. Bear J., Verruijt A. *Modeling Groundwater Flow and Pollution*, D. Reidel, Dordrecht, Holland, 1987.
2. Gunduz O, Aral MM. River networks and groundwater flow: a simultaneous solution of a coupled system. *Journal of Hydrology* 2005; **301**:216–234.
3. Liang D, Falconer RA, Lin B. Coupling surface and subsurface flows in a depth averaged flood wave model. *Journal of Hydrology* 2007; **337**:147–158.
4. Kong J, Xin P, Song Z-y, Li L. A new model for coupling surface and subsurface water flows: With an application to a lagoon. *Journal of Hydrology* 2010; **390**:116–120.
5. Casulli V. A conservative semi-implicit method for coupled surface-subsurface flows in regional scale. *International Journal for Numerical Methods in Fluids* 2015; **79**:199–214.
6. Panday S, Huyakorn PS. A fully coupled physically-based spatially–distributed model for evaluating surface/subsurface flow. *Advances in Water Resources* 2004; **27**:361–382.
7. Kollet SJ, Maxwell RM. Integrated surface–groundwater flow modeling: A free-surface overland flow boundary condition in a parallel groundwater flow model. *Advances in Water Resources* 2006; **29**:945–958.
8. Spanoudaki K, Stamou AI, Nanou-Giannarou A. Development and verification of a 3-D integrated surface water–groundwater model. *Journal of Hydrology* 2009; **375**:410–427.
9. Yuan L-R, Xin P, Kong J, Li L, Lockington D. A coupled model for simulating surface water and groundwater interactions in coastal wetlands. *Hydrological Processes* 2011; **25**:3533–3546.
10. Weill S, Mouche E, Pain J. A generalized Richards equation for surface/subsurface flow modelling. *Journal of Hydrology* 2009; **366**:9–20.
11. Dongfang T, Defu L. A new integrated surface and subsurface flows model and its verification. *Applied mathematical modelling* 2011; **35**:3574–3586.
12. Sulis M, Meyerhoff SB, Paniconi C, Maxwell RM, Putti M, Kollet SJ. A comparison of two physics-based numerical models for simulating surface water–groundwater interactions. *Advances in Water Resources* 2010; **33**:456–467.
13. Casulli V, Zanolli P. A nested Newton type algorithm for finite volume methods solving Richards' equation in mixed form. *SIAM Jour. on Scientific Computing* 2010; **32**:2255–2273.
14. Casulli V. Semi-implicit finite difference methods for the two-dimensional shallow water equations. *Journal of Computational Physics* 1990; **86**:56–74.
15. Casulli V, Cheng RT. Semi-implicit finite difference methods for three-dimensional shallow water flow. *International Journal for Numerical Methods in Fluids*. 1992; **15**:629–648.
16. Casulli V, Cattani E. Stability, accuracy and efficiency of a semi-implicit method for three-dimensional shallow water flow. *Computers & Mathematics with Applications* 1994; **27**:99–112.
17. Casulli V, Walters RA. An unstructured grid, three-dimensional model based on the shallow water equations. *International Journal for Numerical Methods in Fluids* 2000; **32**:331–348.
18. Brugnano L, Casulli V. Iterative solution of piecewise linear systems. *SIAM Journal on Scientific Computing* 2008; **30**:463–472.
19. Brugnano L, Casulli V. Iterative solution of piecewise linear systems and applications to porous media. *SIAM Journal on Scientific Computing* 2009; **31**:1858–1873.

20. Casulli V, Zanolli P. Iterative solutions of mildly nonlinear systems. *Journal of Computational and Applied Mathematics* 2012; **236**:3937–3947.
21. Casulli V. A high-resolution wetting and drying algorithm for free-surface hydrodynamics. *International Journal for Numerical Methods in Fluids* 2009; **60**:391–408.
22. Casulli V, Stelling GS. Semi-implicit subgrid modelling of three-dimensional free-surface flows. *International Journal for Numerical Methods in Fluids* 2011; **67**:441–449.
23. Richards, LA. Capillary conduction of liquids through porous mediums. *Journal of Applied Physics* 1931; **1**:318–333.
24. Brooks RH, Corey AT. *Hydraulic properties of porous media*, Hydrology Paper No.3, Civil Engineering, Colorado State University, Fort Collins, CO, 1964.
25. Van Genuchten MTh. A Closed-form Equation for Predicting the Hydraulic Conductivity of Unsaturated Soils. *Soil Science Society of America Journal* 1980; **44**:892–898.
26. Stelling GS, Duynmeyer SPA. A staggered conservative scheme for every Froude number in rapidly varied shallow water flows. *International Journal for Numerical Methods in Fluids* 2003; **43**:1329–1354.
27. Casulli V. A semi-implicit numerical method for the free-surface Navier-Stokes equations. *International Journal for Numerical Methods in Fluids* 2014; **74**:605–622.
28. Casulli V, Zanolli P. High Resolution Methods for Multidimensional Advection-Diffusion Problems in Free-Surface Hydrodynamics. *Ocean Modelling* 2005; **10**:137–151.
29. Sehili A, Lang G, and Lippert C. High-resolution subgrid models: a background, grid generation, and implementation. *Ocean Dynamics* 2014; **64**:519–535.
30. Wang HV, Loftis JD, Liu Z, Forrest D, Zhang J. The Storm Surge and Sub-Grid Inundation Modeling in New York City during Hurricane Sandy. *Journal of Marine Science and Engineering* 2014; **2**:226–246.
31. Ebrahimi K, Falconer RA, Lin B. Flow and solute fluxes in integrated wetland and coastal systems. *Environmental Modelling & Software* 2007; **22**:1337–1348.
32. Goswami PS, Clement TP. Laboratory-scale investigation of saltwater intrusion dynamics. *Water Resources Research* 2007; **43**:W04418 (1–11).
33. Chang SW, Clement TP. Experimental and numerical investigation of saltwater intrusion dynamics in flux-controlled groundwater systems. *Water Resources Research* 2012; **48**:W09527 (1–10).
34. Povich TJ, Dawson CN, Farthing MW, Kees CE. Finite element methods for variable density flow and solute transport. *Computational Geosciences* 2013; **17**:529–549.
35. Di Giammarco P, Todini E, Lamberti P. A conservative finite elements approach to overland flow: the control volume finite element formulation. *Journal of Hydrology* 1996; **175**:267–291.